RESEARCH ARTICLE

From CO_2 Sequestration to Hydrogen Storage: Further Utilization of Depleted Gas Reservoirs

Jingjuan Wu[1,*] **and Ubedullah Ansari**[2]

[1] School of Material Science and Engineering, Henan Polytechnic University, Jiaozuo 454000, China
[2] Institute of Petroleum & Natural Gas Engineering, Mehran University of Engineering and Technology, Jamshoro 76062, Pakistan

Abstract

The depleted gas reservoirs can serve not only as sites for CO_2 sequestration but also as potential spaces for hydrogen storage. However, this process remains insufficiently understood, limiting the availability of reliable technical guidance for injection operations. In this study, a mathematical model for simulating hydrogen storage in depleted gas reservoirs was developed and numerically solved. Meanwhile, the applicability was then verified through comparison with results from previous studies. Based on this model, a detailed analysis was performed to investigate the evolution of key parameters under specific injection conditions. Finally, the effects of various factors on parameters such as hydrogen distribution and maximum pore pressure during the hydrogen injection process were thoroughly discussed. It was found that hydrogen gradually drives the CH_4 and CO_2 outward from the near-wellbore region, leading to increases in both bottom-hole pressure and pore pressure during hydrogen injection. Furthermore, as the injection progresses, the spatial extent of hydrogen distribution expands nonlinearly, and the buffering effects of CH_4 and CO_2 become prominent. Sensitivity analysis further reveals that, although low permeability-induced high pore pressure poses sealing challenges, limited hydrogen storage space within reservoir is beneficial for further hydrogen recovery. Meanwhile, a moderate increase in the injection rate can enhance storage efficiency without compromising reservoir sealing integrity. In contrast, extending the length of wellbore section used for hydrogen injection does not lead to a significant improvement in storage performance.

Keywords: hydrogen storage, CO_2 sequestration, depleted gas reservoir, CCUS, H_2 injection, clean energy.

1 Introduction

As the world transitions to low-carbon energy systems, hydrogen (H_2) is gaining recognition as an essential element of clean energy infrastructure, attributable to its high energy density and zero-emission combustion [1, 2]. However, hydrogen produced via major current pathways, such as fossil fuel

Submitted: 23 July 2025
Revised: 15 September 2025
Accepted: 17 September 2025
Published: 30 September 2025

Vol. 1, **No.** 1, 2025.
10.62762/RS.2025.860510

***Corresponding author:**
✉ Jingjuan Wu
wjj2020@hpu.edu.cn

Citation
Wu, J., & Ansari, U. (2025). From CO_2 Sequestration to Hydrogen Storage: Further Utilization of Depleted Gas Reservoirs. *Reservoir Science*, 1(1), 19–35.

© 2025 by the Authors. Published by Institute of Central Computation and Knowledge. This is an open access article under the CC BY license (https://creativecommons.org/licenses/by/4.0/).

reforming, often faces temporal and volumetric mismatches with demand, which limits its efficient and continuous utilization [3, 4]. Accordingly, large-scale underground hydrogen storage is emerging as a strategic infrastructure for supporting modern energy systems [5, 6]. It plays a critical role in enhancing the stability and flexibility of energy systems by mitigating this mismatch through effective peak shaving. In parallel, the geological storage of carbon dioxide (CO_2) has emerged as a complementary strategy for climate change mitigation, and the synergistic combination of these two approaches offers a promising pathway toward sustainable energy management.

Meanwhile, geological CO_2 sequestration has been extensively studied and is increasingly implemented worldwide [7–9]. Among various geological formations, depleted gas reservoirs are preferred sites for CO_2 sequestration due to their favorable geological conditions, reliable sealing capacity, and comprehensive existing infrastructure. As these reservoirs are progressively repurposed for CO_2 sequestration, the emergence of "composite reservoirs" comprising injected CO_2 and residual methane (CH_4) becomes inevitable [10, 11]. This type of reservoir not only contributes to carbon reduction objectives but also holds significant potential as a high-quality site for future hydrogen storage. This is because the injected carbon dioxide and residual methane within the reservoir can act as buffer gases. These gases can stabilize reservoir pressure during hydrogen storage and facilitate the regulation of injection–production dynamics [12–14]. Accordingly, hydrogen recovered after short-term geological storage exhibits high purity in the extracted gas mixture as well as high recovery efficiency. Conversely, without the buffering effect of methane and carbon dioxide, the injected hydrogen would rapidly fill the entire reservoir space [15]. In this case, the recovery of the injected hydrogen during H_2 recovery after short-term storage will be significantly reduced. Figure 1 clearly illustrates the utilization of depleted gas reservoirs in CO_2 sequestration and further hydrogen storage. A synergistic integration of carbon management and clean energy storage can be achieved through engineering operations based on the concepts illustrated in Figure 1, with this study specifically focusing on the process represented by the transition from subgraph (b) to subgraph (c).

Numerous researchers have conducted extensive investigations on hydrogen storage in depleted gas reservoirs, which has resulted in substantial progress in this field. Representative examples include the work of Liu et al. [16], who performed numerical simulations to evaluate the feasibility of hydrogen storage in depleted shale gas reservoirs in the Fuling region, China. Although the findings revealed the significant potential for both injection and extraction, the lower hydrogen purity in the produced gas increases the complexity and cost of subsequent separation processes. Muhammed et al. [17] experimentally investigated the role of methane as a buffer gas for hydrogen storage in depleted gas reservoirs. The findings indicate that a methane proportion of 30% to 40% in the depleted reservoirs optimizes the storage and extraction efficiency of hydrogen. Kanaani et al. [18], numerically investigated the efficacy of various buffer gases in hydrogen storage within the depleted oil reservoirs. It was demonstrated that methane outperforms nitrogen and carbon dioxide as a buffer gas, enhancing the efficiency of hydrogen storage and extraction in these reservoirs. He et al. [19] developed a novel model to estimate the capacity of hydrogen storage in depleted gas reservoirs using CO_2 and CH_4 as a buffer gas. The findings demonstrate that employing CO_2 or CH_4 as a buffer gas enhances the storage capacity and the recovery, and a 16% reduction of CO_2 resulting in a 7% increase in the hydrogen in reservoir. Zeng et al. [20] conducted a comprehensive review of the primary challenges associated with integrity during hydrogen storage in depleted gas reservoirs. Based on this analysis, they developed a methodology to evaluate integrity-related risks and uncertainties during hydrogen storage, facilitating informed decision-making for selecting optimal underground hydrogen storage pilot projects in these reservoirs. Undoubtedly, these studies provide valuable insights for estimating storage capacity, selecting suitable sites, and evaluating associated risks in hydrogen storage within depleted gas reservoirs. However, current research on this topic still exhibits several limitations and gaps that require further investigation. Firstly, most of these investigations frequently employ a single gas, such as methane or CO_2, as a buffer gas for hydrogen storage in depleted gas reservoirs. In other words, studies specifically addressing hydrogen injection behavior in depleted gas reservoirs previously used for CO_2 sequestration remain scarce. Secondly, the majority of current research is based on vertical well models, whereas fluid flow dynamics during hydrogen injection via horizontal wells have received little attention [21,

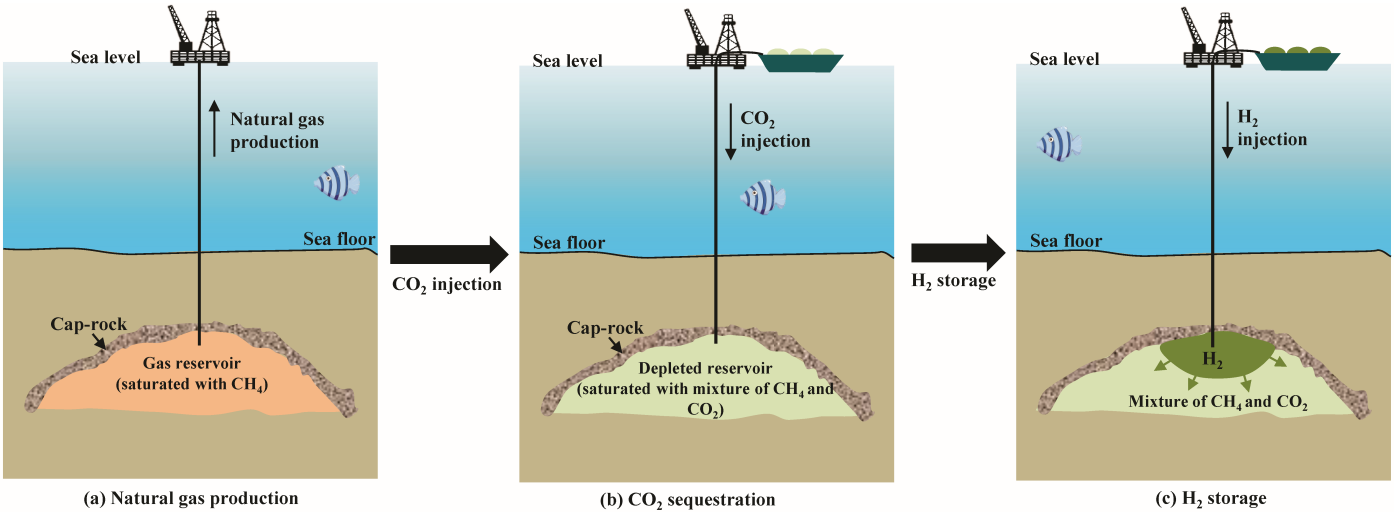


Figure 1. Utilization process of depleted gas reservoirs in CO_2 sequestration and further hydrogen storage.

22]. These research gaps provide the foundation for conducting pertinent studies in the present work.

Inspired by the previous investigations, an investigation model for hydrogen injection into depleted gas reservoirs pre-stored with CO_2, using a dual-horizontal-well configuration, was developed. Based on the model, the flow behavior of multi-component gases in the depleted reservoir during hydrogen injection process was analyzed. Meanwhile, a sensitivity analysis was performed to investigate the behavior of the hydrogen diffusion front. This study aims to establish a theoretical foundation for the engineering design and operational control of hydrogen injection into CO_2-sequestered depleted reservoirs.

To better facilitate comprehension, the principal highlights of this study are outlined as follows:

1. The feasibility of utilizing depleted gas reservoirs previously employed for CO_2 sequestration as sites for hydrogen storage was explored through comparative analysis, with attention to both engineering considerations and sustainable development.

2. The behavior of different gas-phase components (i.e., CO_2, CH_4 and H_2) during hydrogen injection into depleted gas reservoirs that had been pre-sequestered with CO_2 was investigated.

3. The influence of various factors on hydrogen storage and the stability of the storage formation was analyzed.

2 Numerical model

In this section, a systematic modeling framework is presented, encompassing the governing equations, the equations of state, and the specification of well control parameters. Furthermore, the model implementation and validation of its applicability are also discussed. The following assumptions were adopted in the development of the mathematical model for this study. (1) It was assumed that water and gas coexist within the reservoir, neglecting complex thermodynamic effects, such as gas dissolution into the oil phase. (2) Parameters such as the density and viscosity of the water phase are assumed to be constant, independent of factors such as pressure and temperature. (3) The reservoir in the model is a closed system in which mass exchange occurs solely through the wells. (4) The physical properties of the sediment within the model are assumed to be homogeneous and isotropic. (5) It was assumed that the sediment temperature remains constant, neglecting thermal effects induced by operations such as hydrogen injection. All these represent the primary assumptions, though they do not encompass all assumptions considered. However, these assumptions are deemed sufficient for the purposes of the simulation conducted in the present work.

2.1 Governing and Auxiliary Equations

In the present work, the injection dynamics of two-phase (water and gas) and three-component gas mixture (H_2, CH_4, and CO_2) within a three-dimensional depleted reservoir was simulated. For such a fluid system, the mass conservation equation for each component is formulated as

follows [23]:

$$\begin{cases} \dfrac{\partial}{\partial t}\left(\phi \sum\limits_{\alpha} x_{i,\alpha}\rho_{\alpha}S_{\alpha}\right) + \nabla\left(\sum\limits_{\alpha} x_{i,\alpha}\rho_{\alpha}v_{\alpha}\right) = q_i + \Gamma_i \\ \Gamma_i = k_i a\left(c_i^{w,eq} - c_i^{w}\right) \end{cases} \tag{1}$$

where ϕ is the porosity of reservoir in %, $x_{i,\alpha}$ is the mole fraction of component i in phase α in %, ρ_α is the density of phase α in kg/m^3, S_α is the saturation of phase α in %, v_α is the Darcy flow velocity of phase α in m/s, q_i is the source and/or sink term of component i in kg/(m^3.s), Γ_i is the mass transfer term between phases in mol/(m^3.s), k_i is the mass transfer rate constant in m/s, a is phase interface area density in 1/m, $C_i^{w,eq}$ is the equilibrium concentration of water.

The flow of each phase follows Darcy's law, and the flow velocity v$_\alpha$ can be expressed as

$$v_\alpha = -\frac{k_{r\alpha}}{\mu_\alpha} K\left(\nabla p_\alpha - \rho_\alpha g\right) \tag{2}$$

where k_α is the relative permeability of phase α, μ_α is the viscosity of phase α in Pa·s, K is the absolute permeability in mD, p_α is the pressure of phase α in Pa, g is the gravity acceleration vector in m/s^2.

The relative permeability is defined using the Corey model, and the relative permeability of gas and water can be expressed as

$$\begin{cases} k_{rw} = \left(\dfrac{S_w - S_{wr}}{1 - S_{wr} - S_{gr}}\right)^{n_w} \\ k_{rg} = \left(\dfrac{S_g - S_{gr}}{1 - S_{gr} - S_{wr}}\right)^{n_g} \end{cases} \tag{3}$$

where S_{wr} and S_{gr} are the residual water saturation and residual gas saturation, respectively. n_w and n_g are the Corey exponents for water and gas, respectively. These functions account for the nonlinear variation of relative permeability with saturation while incorporating the effects of residual saturation. These functions account for the nonlinear variation of relative permeability with saturation while incorporating the effects of residual saturation.

The distribution of each component in the gas phase is closely related to the thermodynamic conditions of the reservoir, including pressure, temperature, and fluid properties such as solubility and capillary effects [24, 25]. To capture these phase behaviors, phase equilibrium calculations are performed using an Equation of State (i.e., EOS). Herein, an enhanced Peng-Robinson Equation of State (PR-EOS) was employed, which was written as the following form as

$$\begin{cases} p = \dfrac{RT}{V-b} - \dfrac{a(T)}{V(V+b)+b(V-b)} \\ a(T) = 0.457\dfrac{R^2T_c^2}{P_c}\alpha(T) \\ b = 0.078\dfrac{RT_c}{P_c} \\ \alpha(T) = \Big[1 + \big(0.37464 + 1.54226\omega \\ \qquad - 0.26992\omega^2\big)\cdot\Big(1 - \Big(\dfrac{T}{T_c}\Big)^{0.5}\Big)\Big]^2 \end{cases} \tag{4}$$

where V is molar volume in m^3/mol, R is the universal gas constant (8.314 J/(mol·K)), T is temperature in °C, p_c is the critical pressure in Pa, T_c is the critical temperature in °C, ω is the acentric factor.

The development of the numerical model necessitates the incorporation of some additional auxiliary equations. The aforementioned assumption posits that the pores of the investigation model are fully saturated with water and gas. This two-phase configuration is consistent with observed wettability characteristics of hydrogen/brine/rock systems and field evidence from depleted gas reservoirs where water and gas coexist as the primary pore-filling fluids [26, 27]. Consequently, the following relationship exists between the saturation of the water and gas phases:

$$S_g + S_w = 1 \tag{5}$$

Furthermore, the gas phase comprises three components: H_2, CO_2, and CH_4. Consequently, the relationship of volume fraction among these three gas components satisfies the following equation:

$$\sum_i x_{i,a} = 1 \quad \forall a \tag{6}$$

2.2 Initial and boundary conditions

To facilitate the definition of boundary and initial conditions, Figure 2 illustrates the geometric model employed for numerical simulations of H_2 injection and storage. As depicted in Figure 2, the geometric model is a three-dimensional one with dimensions of 800 m in length, 800 m in width, and 600 m in height. In the simulation, hydrogen is continuously injected at a constant rate into the depleted reservoir model through two horizontal wells. Due to the buffering effect of residual CH_4 and previously stored CO_2 in reservoir, the injected hydrogen (H_2) is constrained

to a confined region around the wellbore. To facilitate numerical simulation, the numerical model depicted in Figure 2 is discretized into 40, 40, and 30 elements along the three respective spatial directions. That is to say, there are a total of 48000 elements in the model.

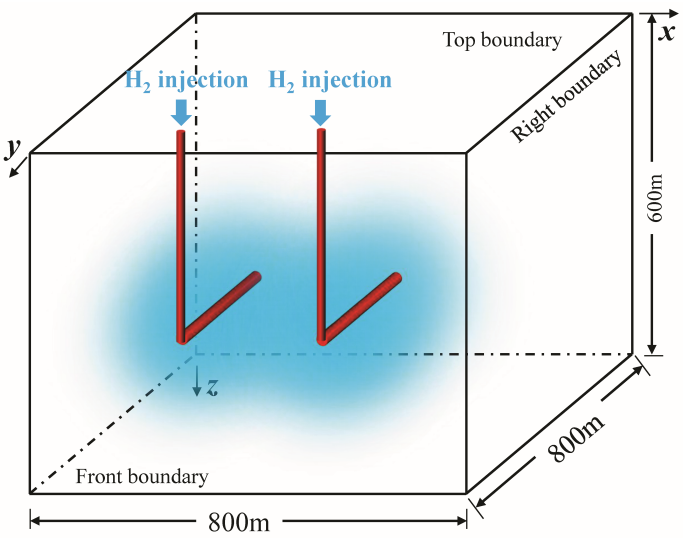


Figure 2. Geometric model for numerical simulation of H_2 injection and storage in depleted reservoir.

The Neumann boundary conditions (i.e., no-flow conditions) were applied in the model, ensuring that no mass transfer occurs across any of its boundaries, which can be expressed as

$$v_\alpha \cdot n = 0 \quad \text{on} \quad \partial\Omega \tag{7}$$

where n is the normal vector of the element boundary, Ω is the outer boundaries of the numerical model (including the top, bottom, front, back, left and right sides).

The simulation conducted in this study is the pure multi-component seepage analysis occurring between two phases. Therefore, the initial conditions primarily encompass the spatial distribution definitions for pore pressure, temperature, and phase saturation. For the initial pore pressure, it is assumed to vary linearly with depth and can be expressed as follows:

$$p = p_{\text{ref}} + \rho g(z - z_{\text{ref}}) \tag{8}$$

where p_{ref} and z_{ref} are the reference pressure and reference depth respectively, corresponding to the pressure and depth at the top boundary.

Correspondingly, the temperature distribution can be represented as

$$T = T_{\text{ref}} + dT(z - z_{\text{ref}}) \tag{9}$$

where T_{ref} is the reference temperature, dT is the geothermal gradient in °C/m.

The initial distribution of gas and water saturation throughout the entire model is defined as

$$S = [S_{wi}, S_{gi}] \tag{10}$$

where S_{wi} and S_{gi} are the initial water and gas saturation respectively.

The initial molar fractions of H_2, CH_4, and CO_2 in the gas phase are specified as

$$x = [x_{\text{H}_2 i}, x_{\text{CH}_4 i}, x_{\text{CO}_2 i}] \tag{11}$$

where $x_{\text{H}_2 i}$, $x_{\text{CH}_4 i}$, and $x_{\text{CO}_2 i}$ are the initial molar fractions of H_2, CH_4, and CO_2 respectively.

During the injection phase, fluid flow is primarily governed by the well control conditions imposed in the model. Herein, the injection of H_2 is implemented through a constant rate, which is written as

$$q_{i,\text{inj}} = \begin{cases} q_{\text{inj}} \cdot x_{i,\text{inj}} & \text{Wellbore} \\ 0 & \text{Other element} \end{cases} \tag{12}$$

where $q_{i,\text{inj}}$ is the injection rate of component i, $x_{i,\text{inj}}$ is the molar fraction of component i in injection fluid, and q_{inj} is the total injection rate.

2.3 Model implementation and applicability verification

In this study, the finite volume method was utilized to numerically solve the proposed mathematical model. In this section, the mass conservation equation, the Darcy's law, and the corresponding boundary and initial conditions are discretized in detail across the temporal and spatial domains.

For the mass conservation equation, the discretized form is:

$$\frac{(\phi \sum_\alpha x_{i,\alpha}\rho_\alpha S_\alpha)^{n+1} - (\phi \sum_\alpha x_{i,\alpha}\rho_\alpha S_\alpha)^n}{\Delta t} + \nabla \cdot \left(\sum_\alpha x_{i,\alpha}^{n+1} \rho_{i,\alpha}^{n+1} v_{i,\alpha}^{n+1} \right) = q_i^{n+1} + \Gamma_i^{n+1} \tag{13}$$

where Δt is the time increment in days, and n is the number of time steps.

For any investigated element Ω_k, the volume-integrated form of the mass conservation

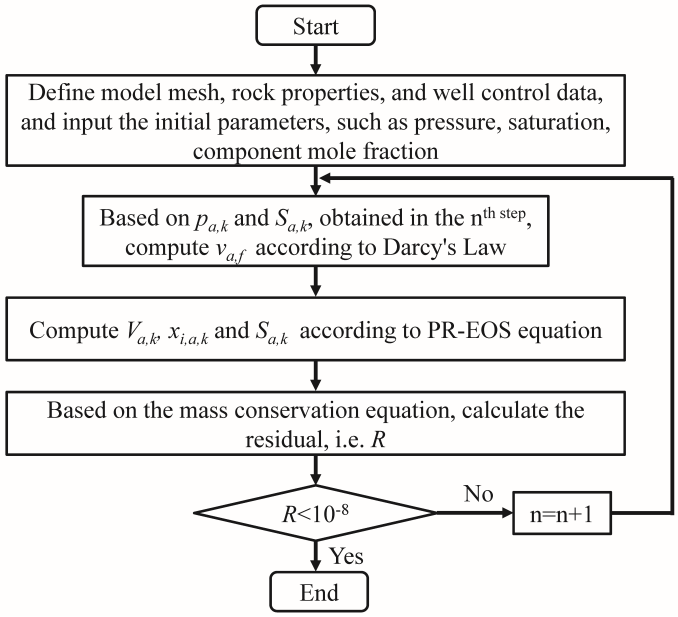


Figure 3. The implementation workflow.

equation can be expressed as follows:

$$\int_{\Omega_k} \frac{\partial}{\partial t}\left(\phi \sum_{\alpha} x_{i,\alpha}\rho_{\alpha}S_{\alpha}\right) dV + \int_{\Omega_k} \nabla \cdot \left(\sum_{\alpha} x_{i,\alpha}\rho_{\alpha}v_{\alpha}\right) dV = \int_{\Omega_k} (q_i + \Gamma_i)\, dV \tag{14}$$

After further organization, the discretized form in the spatial domain is expressed as follows:

$$\frac{V_k}{\Delta t}\left(\phi_k \sum_{\alpha} x_{i,\alpha,k}^{n+1}\rho_{\alpha,k}^{n+1}S_{\alpha,k}^{n+1} - \phi_k \sum_{\alpha} x_{i,\alpha,k}^{n}\rho_{\alpha,k}^{n}S_{\alpha,k}^{n}\right) + A_f \sum_{\alpha} (x_{i,a,f}\rho_{\alpha,f}v_{\alpha,f} \cdot \mathbf{n}_f) = V_k q_{i,k} \tag{15}$$

where k is the number of the investigated element, V_k is the volume of element k, and A_f is the area of surface f, n_f is the normal vector of surface f.

The final discretized form of Darcy's law can be expressed as

$$v_{\alpha,f}^{n+1} \cdot n_f = -\frac{k_{\alpha,r,f}^{n+1} \cdot A_f K_f}{\mu_\alpha d_{kl}}\left(\left(p_{\alpha,l}^{n+1} - p_{\alpha,k}^{n+1}\right) - \rho_{\alpha,f}^{n+1} g\,(z_l - z_k)\right) \tag{16}$$

where d_{kl} is the distance between the centers of element k and element l, z_l and z_k are the depth coordinates of element k and element l.

Based on the above-mentioned mathematical model and its discrete form, Figure 3 presents the corresponding implementation workflow and methodology. As illustrated in Figure 3, the solution and implementation of the mathematical model involves a multi-step computational process. The feasibility of the investigation methodology proposed in this study was assessed by verifying its applicability against results from previous simulation studies. In this study, the investigation conducted by Lu et al. [28] was used as a reference for comparison. According to the investigation model and injection strategy used in Lu et al. [28], H_2 injection simulation was conducted, and the comparison of simulation results is shown in Figure 4.

As depicted in Figure 4, the hydrogen saturation distributions obtained from the two simulations exhibit a high degree of similarity, both in spatial patterns and in overall range. In both cases, the injected hydrogen is mainly confined within a reservoir approximately 300 m thick located in the upper part of the model. The storage region shows a characteristic pancake-like geometry, with a thicker central zone that tapers toward the edges. The radial extent of the hydrogen saturation front reaches 897 m in the reference study [28], whereas the methodology proposed here yields a slightly smaller extent of 821 m. This discrepancy can be attributed primarily to the simplified assumption of homogeneous and isotropic sediments in our model, in contrast to the normally distributed permeability considered in the referenced work. Furthermore, the slightly smaller element size adopted in this study may also contribute to the observed difference shown in Figure 4. Nevertheless, the high similarity between the two results in Figure 4 can still confirm the applicability of the proposed mathematical model and methodology for simulation of hydrogen storage in depleted gas reservoir. The relative deviation in the radial extent of the hydrogen saturation front between the two methods is approximately 8.5% (897 m vs. 821 m), which falls within an acceptable range for engineering applications given the differences in model assumptions.

3 Injection Behavior During the H_2 Injection Process

3.1 Basic data for simulation

Appropriate basic data serve as the foundation and prerequisite for numerical simulations of hydrogen storage. The parameters required for hydrogen storage in depleted gas reservoirs primarily include those related to reservoir properties, pore fluid

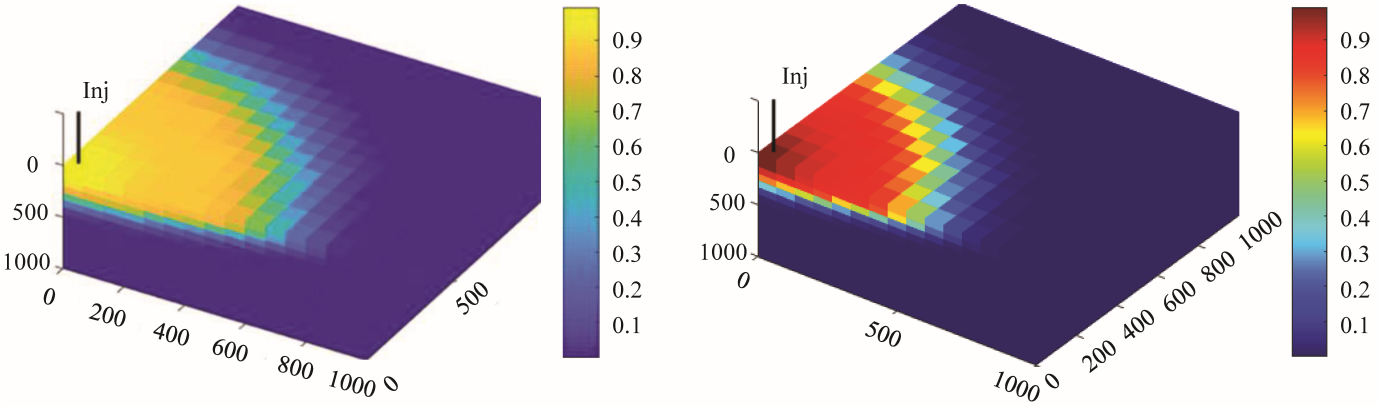


Figure 4. Comparison of H_2 saturation distribution obtained by Lu et al. [28] and that obtained by the investigation method in this study.

Table 1. Basic parameters used for simulation (default case).

Parameter	Unit	Value	Parameter	Unit	Value
Water viscosity	mPa·s	1.0	Initial water saturation	%	0
Water density	kg/m^3	1030	Initial gas saturation	%	100
Gas viscosity	mPa·s	8×10^{-3}	Initial xg,H_2	-	0
Gas density	kg/m^3	Determined by EOS	Initial xg,CO_2	-	0.9
Permeability	mD	5.0	Initial xg,CH_4	-	0.1
Porosity	%	10	Injected xg,H_2	-	1
Model geometry	m	800×800×600	Initial pore pressure	Pa	Equation (8)
Element assignment		40×40×30	Initial temperature	℃	Equation (9)
Total time	Year	0.5	Injection rate	m^3/day	2.25×10^6
Residual gas saturation	%	10	Time increment	Day	10
Critical pressure, Pc	MPa	CH_4: 4.599 CO_2: 7.377 H_2: 1.297	Critical temperature, Tc	K	CH_4: 190.56 CO_2: 304.13 H_2: 33.19
Model depth	m	1000	Injection style	Equal devised by 2 wells	
Length of wellbore	m	400	Wellbore depth	m	300

characteristics, and injection engineering, which were listed in Table 1. Notably, sensitivity analysis can be performed by appropriately modifying the relevant parameters listed in Table 1.

In this study, a case in which hydrogen, produced but not immediately required, can only be stored by injection into a depleted gas reservoir was investigated. Therefore, the simulation duration was 0.5 year herein, without employing a mode of alternating injection and extraction.

3.2 Dynamic analysis during hydrogen injection

The injection of hydrogen into depleted reservoir inevitably induces a continuous variation in bottom-hole pressure and pore pressure. Thus, Figure 5 illustrates the variations in pore pressure within the model and bottom-hole pressure over a six-month period of hydrogen injection. As depicted in Figure 5(a), the pore pressure in the near-wellbore region increases instantaneously at the beginning of injection operation. At this stage, the pore pressure disturbance induced by hydrogen injection is primarily confined to the area around wellbore. As the injection operation proceeds, the disturbance caused by hydrogen injection on the pore pressure within the model becomes increasingly pronounced. After 135 days of injection, the pore pressure within the model had essentially reached a state of equilibrium. Even with continued hydrogen injection beyond this time, the pore pressure within the model exhibits negligible variation. Based on mechanical analysis, the fracture pressure of the reservoir is 20 MPa. It can also be seen from Figure 5(a) that the maximum pressure within the model reaches 5.78 MPa throughout the simulation, which remains within the safe operational limits for the reservoir. This is attributed to the fact that the maximum pore pressure remains well below the reservoir's fracture pressure. It can be inferred that, from the perspective of reservoir integrity/stability, further increases in the hydrogen injection rate are feasible, and this will be analyzed in detail later in this manuscript. During hydrogen injection, the bottom-hole pressure will also increase accordingly. As observed in Figure 5(b), the bottom-hole pressure in both horizontal wells gradually increases during H_2 injection operation, but the increasing trend of bottom-hole pressure gradually slows down. The

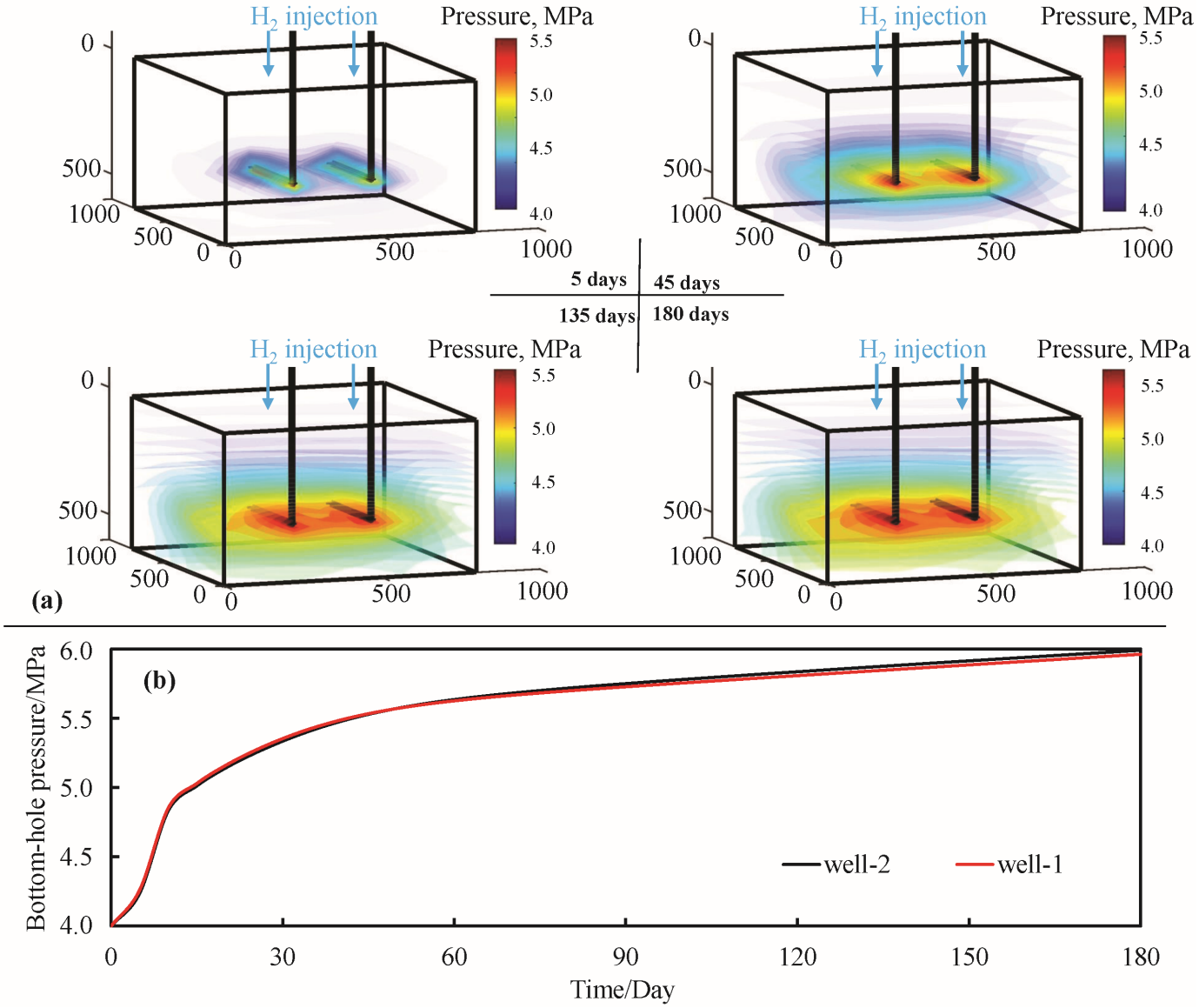


Figure 5. Variation of (a) pore pressure and (b) bottom-hole pressure during H_2 injection over 0.5 year.

final bottom-hole pressures of the two injection wells reached 5.99 MPa and 5.96 MPa, respectively, which are still lower than the fracture pressure of the reservoir. This indicates that the integrity of both wellbore can also be maintained at this default injection rate.

Figure 6 presents the evolution of mole fraction distributions for H_2, CO_2, and CH_4 within the investigation model during the injection operation. As illustrated in Figure 6, with the injection of hydrogen, the CO_2 and CH_4 that were originally distributed around the wellbore are gradually displaced outward, away from the injection point. The sediment pores in the near-wellbore region are primarily occupied by injected hydrogen. During this process, the mole fraction of hydrogen increases progressively, while those of methane and carbon dioxide decrease rapidly until they approach zero. Due to the presence of CH_4 and CO_2 in the depleted gas reservoirs, the diffusion of hydrogen is markedly inhibited. After 135 days of injection, the hydrogen injected through the two horizontal wells begins to converge and continues to expand within the reservoir. By the end of the injection operation, the injected hydrogen had nearly reached the lateral boundaries of the investigation model but was still far from the vertical boundaries. This is attributed to the reservoir's vertical permeability being lower than its horizontal permeability, a characteristic rooted in the depositional fabric and petrophysical properties of reservoir sandstones [21, 29, 30]. Although high reservoir permeability facilitates hydrogen injection and storage, it can negatively affect the purity of hydrogen during subsequent recovery.

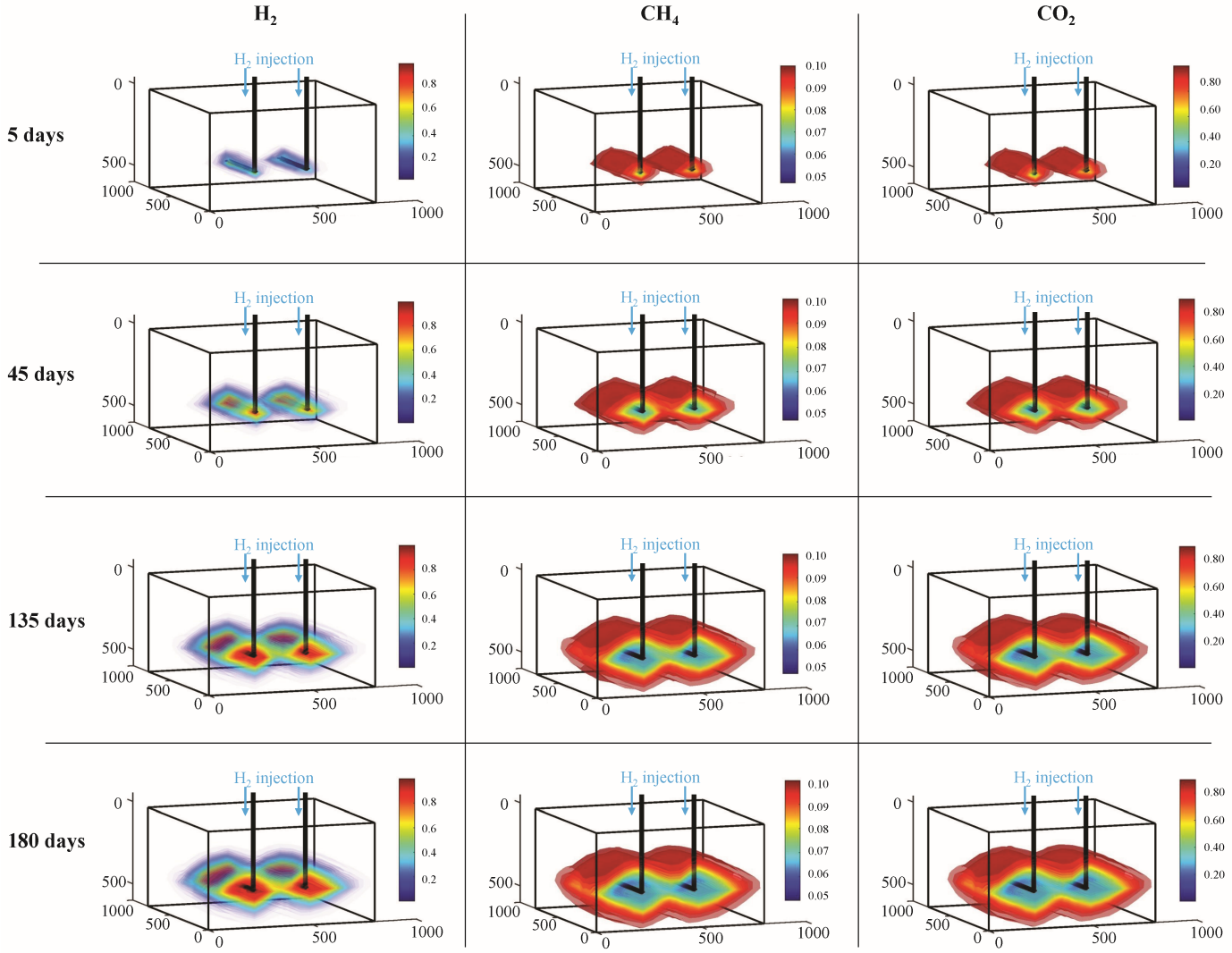
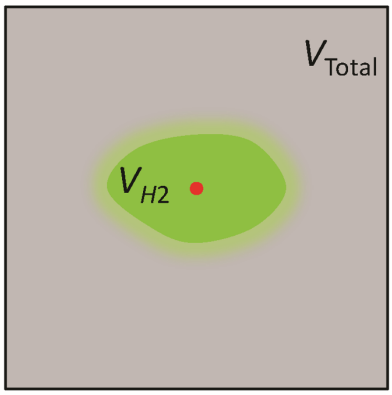


Figure 6. Evolution of mole fractions of H_2, CH_4 and CO_2 during H_2 injection.



(a) Schematic diagram of hydrogen diffusion

```
% === Original grid information===
X_H2 = state{end}.components(:, 1); % H2 mole fraction
cell_volumes = G.cells.volumes; % Volume of each grid cell
total_cells = G.cells.num; % Total number of elements
total_volume = sum(cell_volumes); % Total volume of the model

% === Find out the hydrogen diffusion area===
idx_H2 = find(X_H2 > thresh); % Index of cells with volume
fraction above the concentration threshold
num_cells_H2 = numel(idx_H2); % Number of elements
percent_cells_H2 = num_cells_H2 / total_cells * 100;

% === Calculate the actual H₂ filling volume===
% Perform volume accumulation for units that meet the condition of
X_H2 being higher than the threshold
volume_H2 = sum(cell_volumes(idx_H2) .* X_H2(idx_H2)); % H2 Actual
filling volume (m³)
percent_volume_H2 = volume_H2 / total_volume * 100; % Storage ratio
```

(b) Key code for determining the parameter of "Storage Ratio"

Figure 7. Determination of the parameter "Storage Ratio".

For the purpose of quantitative analysis, a new evaluation parameter termed "storage ratio" (represented as ε) is introduced in this study and defined as the ratio of the hydrogen-occupied volume to the total reservoir volume. Figure 7 presents a schematic diagram of the diffusion of injected hydrogen and the code for solving the "Storage ratio". For the same injection volume of hydrogen, a lower storage ratio indicates a more significant buffering effect for CO_2 and CH_4. The evolution curve of storage ratio during the injection process was presented as Figure 8. As can be seen in

Figure 8, the diffusion of injected hydrogen, which predominantly occurs during the early stage, results in a rapid increase in the storage ratio. After 90 days of injection operation, the storage ratio reached 9.62%. This indicates that the reservoir volume occupied by the injected hydrogen has accounted for 9.62% of the total reservoir volume. It should be noted that the final storage ratio is only 11.82%, with 81.39% of this total being achieved during the first half of the injection period. This also implies that hydrogen injection during the latter half of the operation contributed to only a modest increase of 2.20% in the storage ratio. This is because, in the later stages of the injection operation, the pore pressure within the reservoir is high, and additional hydrogen injection must overcome greater resistance to further diffuse into the reservoir. For comparison, the case where there is no CO_2 sequestration in the reservoir before its use for hydrogen storage was also simulated. The simulation results indicated that the final storage ratio (denoted as ε) could reach as high as 24.05% in the absence of prior CO_2 sequestration in the reservoir (see Figure 8). As previously discussed, the strategy of carbon sequestration before using depleted gas reservoirs for hydrogen storage is advantageous for hydrogen recovery (both in terms of purity and production) following short-term storage.

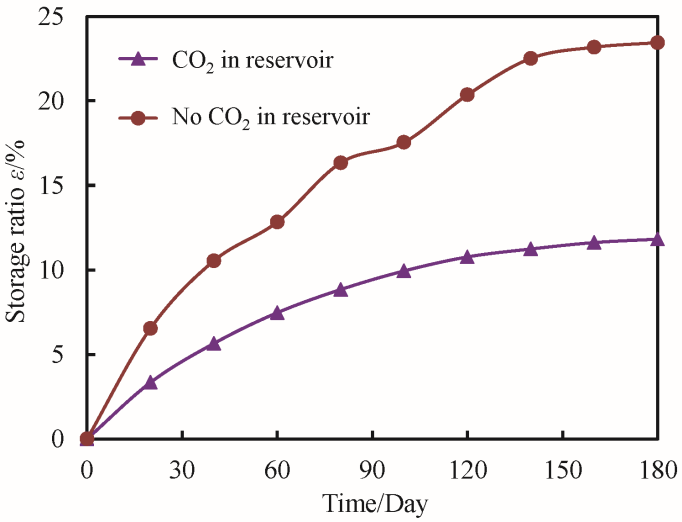


Figure 8. Evolution of parameter ε in the H_2 injection operation when the depleted gas reservoirs was pre-stored with CO_2 or not.

To highlight the buffering effect of carbon dioxide on hydrogen storage in depleted gas reservoirs with pre-stored carbon dioxide, the evolution curve of the storage ratio in the absence of CO_2 is also presented in Figure 8. As shown in Figure 8, in the absence of pre-stored carbon dioxide in the depleted gas reservoir, the final storage ratio exceeds twice that observed when carbon dioxide is pre-stored. The storage ratio of hydrogen was 24.05% when CO_2 sequestration was not performed prior to H_2 injection, but it decreased to 11.82% when CO_2 had been previously stored in the depleted gas reservoir. It is well established that a lower storage ratio corresponds to reduced diffusion of hydrogen injected into the gas reservoir. Therefore, the comparison results presented in Figure 8 demonstrate that prior CO_2 sequestration in depleted gas reservoirs significantly enhances the containment of injected hydrogen by mitigating its diffusion. In other words, the stored CO_2 in depleted gas reservoirs exerts a clear buffering effect on the diffusion of injected hydrogen. The buffering effect of CO_2 can be attributed to the following two aspects. For one thing, CO_2 dissolves in water and undergoes mineralization during the long-term sequestration, resulting in reduced permeability of the gas reservoir. Consequently, the hydrogen injected into the gas reservoir faces more challenges or resistance in diffusing into the sediment located far from the wellbore. For another, the filling of CO_2 into the gas reservoir elevates pore pressure to varying extents. During hydrogen injection, this pressure generates a resistive force that impedes the diffusion and migration of hydrogen [31]. From this perspective, the presence of CO_2, caused by presequestration of CO_2, is critical for enhancing the purity of hydrogen in subsequent hydrogen recovery initiatives.

4 Sensitivity analysis

In this section, the ratio of hydrogen storage volume to total reservoir volume (i.e., ε) was employed as an evaluation parameter to assess the influence of factors such as reservoir permeability and wellbore length. Meanwhile, the mechanisms by which these factors influence the effectiveness of hydrogen sequestration were also discussed. Notably, sensitivity analysis can be implemented by changing the default parameters in the simulation code corresponding to the investigated factors.

4.1 Effect of reservoir permeability

Reservoir permeability plays a crucial role in controlling the migration and diffusion behavior of injected hydrogen, thereby directly affecting underground storage efficiency and reservoir stability. The storage ratios under different reservoir permeability conditions are presented in Figure 9. The results show that the storage ratio gradually decreases with decreasing permeability of the depleted reservoir.

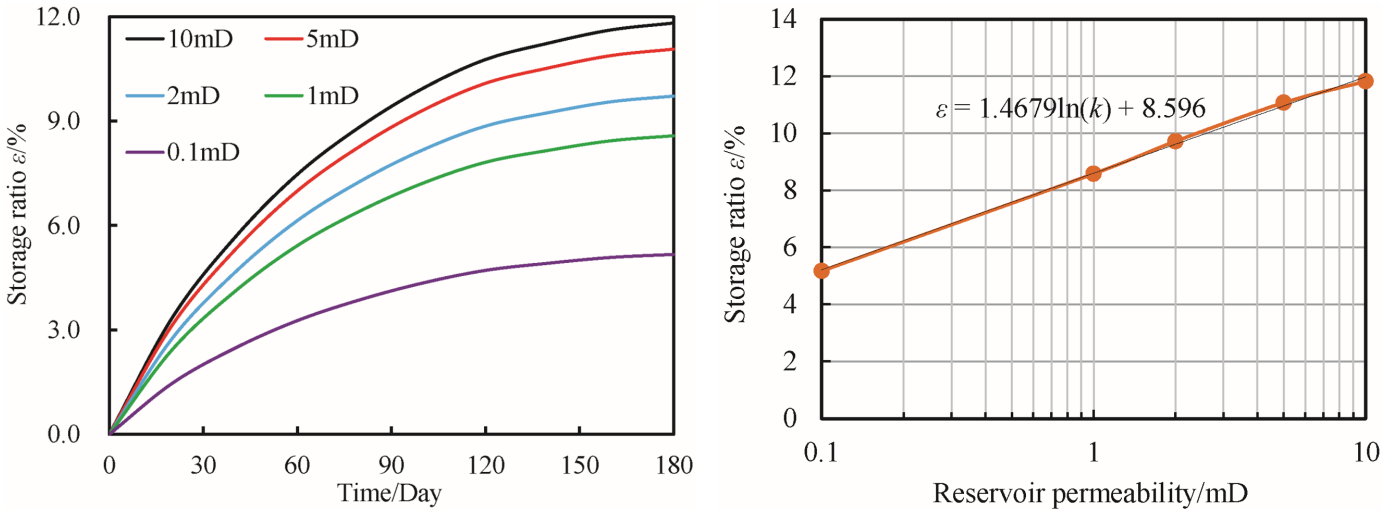


Figure 9. Evolution of parameter ε in the H_2 injection operation.

The storage ratio is 11.82% when the reservoir permeability is 10mD. However, when the depleted gas reservoir exhibits low permeability, the storage ratio decreases sharply, following a logarithmic trend. When the permeability is 0.1 mD, the final storage ratio reaches 5.17%. The relationship between the final storage ratio and reservoir permeability can be expressed through the following fitted equation:

$$\varepsilon = 1.46791 \ln(k) + 8.596 \quad (17)$$

This phenomenon can be attributed to the fact that the CH_4 and CO_2 originally occupying these pore spaces and throats are progressively driven further away from the injection point during hydrogen injection. In a gas reservoir with lower permeability, the seepage pathways are fewer and narrower. Then, these CO_2 and CH_4 exert significant counterforce on the injected hydrogen, thereby impeding its further diffusion within the reservoir. In such case, the injected hydrogen tends to be "locked" within a limited spatial region, and the buffering effects exerted by the pre-existing CH_4 and CO_2 are pronounced. However, in high-permeability reservoirs, the internal seepage paths are more extensively developed and possess larger apertures. The injected hydrogen can easily "push" the CH_4 and CO_2 initially occupying the pore spaces or throats, driving them toward more distal regions of the reservoir. In addition, as shown in Figure 9, the simulation results also indicate that variations in reservoir permeability lead to more pronounced changes in the storage ratio within the low-permeability range. As the reservoir permeability increases from 0.1 mD to 2.0 mD, the storage ratio increases from 5.17% to 9.72%, representing a relative enhancement of approximately 88.01%. However, if the reservoir permeability was increased from 2.0 mD to 10.0 mD, the storage ratio rose from 9.72% to 11.82%, corresponding to a relative increase of only 21.60%. Moreover, it can be inferred that if the permeability of the reservoir continues to increase on the basis of the default permeability, the increase in storage ratio will continue to decrease.

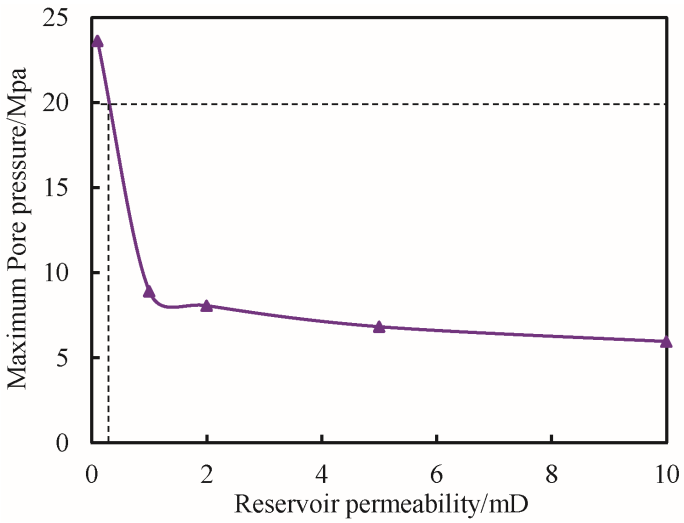


Figure 10. The maximum pore pressure when reservoir permeability is different.

The above analysis clearly demonstrates that CH_4 and CO_2 exhibit a pronounced buffering effect in low-permeability gas reservoirs. However, the increase in pore pressure during gas injection may pose significant risks to the integrity of reservoir and wellbore. Fractures may develop once the reservoir pressure exceeds the fracture pressure, potentially compromising the buffering effects of CO_2 and CH_4 and impairing the reservoir's sealing integrity. In other words, the maximum pore pressure during

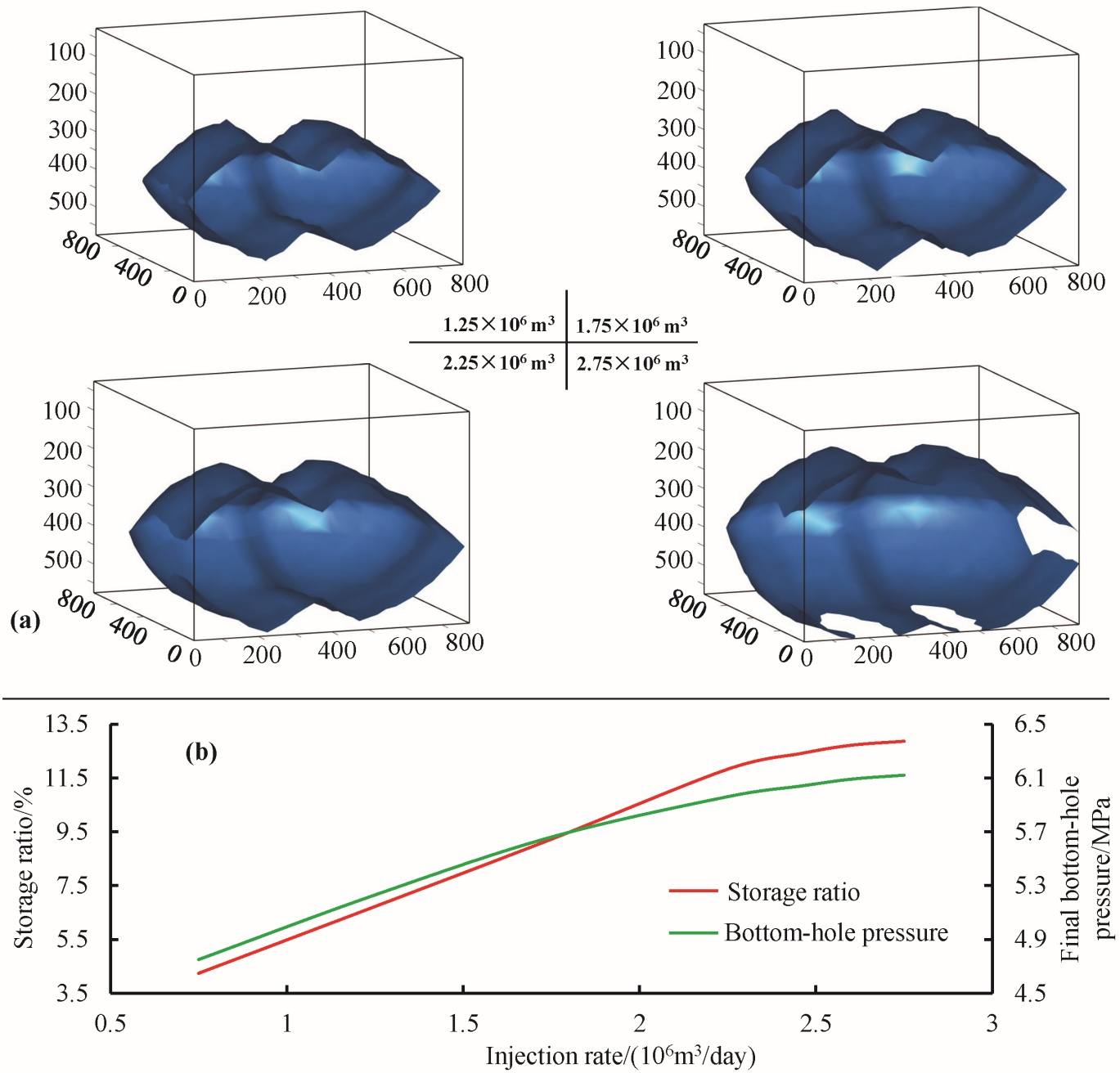


Figure 11. Effect of injection rate on hydrogen storage. (a) Boundary of the final hydrogen distribution area; (b) Storage ratio.

injection must remain below the fracture pressure. Therefore, the reservoir pressure distribution under different permeability conditions was investigated, and the results are presented in Figure 10. The results show that, with increasing reservoir permeability, the maximum reservoir pressure initially decreases rapidly in the low-permeability range and then gradually stabilizes in the high-permeability range. In this study, the permeability threshold at which notable changes in maximum pore pressure occur is approximately 1.0 mD. However, this finding has limited practical relevance to the design and operational control of hydrogen storage projects. To illustrate this constraint, a horizontal dashed line representing the fracture pressure is plotted in Figure 10. The results show that this dashed line intersects with the corresponding curve (i.e., the purple solid line), and the permeability value at the intersection point is 0.2 mD. This indicates that, for the parameter configuration of the current injection project, hydrogen storage is not feasible if the reservoir permeability is below 0.2 mD. If hydrogen injection is to be implemented, alternative strategies—such as reducing the injection rate and extending the

injection section length—must be adopted to mitigate the maximum pore pressure within the reservoir.

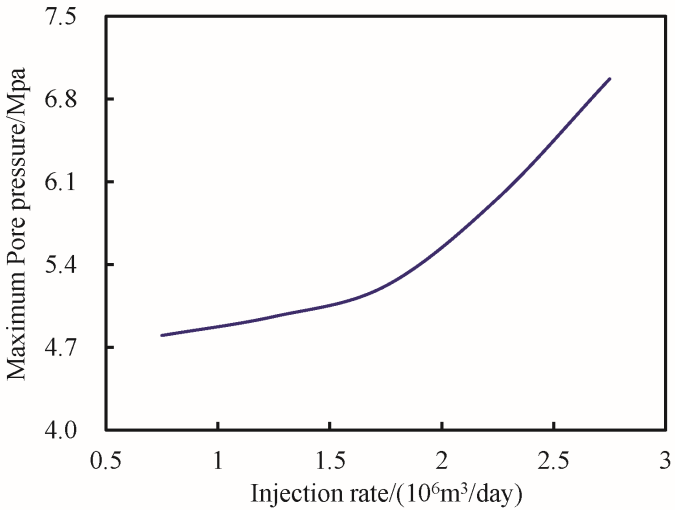


Figure 12. Effect of injection rate on maximum pore pressure.

4.2 Effect of injection rate

The injection rate is also a critical factor influencing the performance of hydrogen storage. An optimized injection rate contributes to improved storage performance without compromising the sustainability of injection operations. This section, therefore, focuses on evaluating the impact of injection rate on hydrogen storage and identifying an optimal rate that ensures reservoir integrity. Herein, the effect of injection rates, varying from 0.75×10^6 to 2.75×10^6 m^3/day, was investigated.

Figure 11 presents the reservoir's hydrogen-filled boundary contours and associated storage ratios at various injection rates. From Figure 11(a), it can be clearly observed that an increase in the hydrogen injection rate leads to a substantial expansion in the volume of the reservoir occupied by injected hydrogen. The quantitative relationship between the injection rate and storage efficiency, as shown in Figure 11(b), further confirms this pattern. When the injection rate of hydrogen is 0.75×10^6 m^3/day, distribution of the injected hydrogen within the reservoir is largely restricted to the vicinity of the two horizontal boreholes. At this injection rate, the corresponding storage ratio is only 4.24%. The boundary of the hydrogen distribution area has not extended to any boundaries of the investigation model. When the injection rate is increased to 1.55×10^6 m^3/day, the boundary of the hydrogen distribution region extends to the left boundary of the model. The storage ratio corresponding to this injection rate is 8.78%. As the injection rate continues to increase, the hydrogen distribution region extends beyond the model boundary, with the injected hydrogen diffusing into areas outside the model (see Figure 11(a)). When the injection rate reaches 2.75×10^6 m^3/day, the front, left, right, and bottom boundaries of the hydrogen distribution region extend beyond the model boundaries, and the storage ratio is as high as 12.86%. This storage ratio is more than 3 times as large as that achieved at an injection rate of 0.75×10^6 m^3/day. This simulation result can be attributed to the fact that higher injection rates lead to elevated bottom-hole pressures, which provide a greater driving force for hydrogen diffusion and migration into the reservoir [22, 32, 33]. As observed in Figure 11(b), the trends of bottom-hole pressure and storage ratio with respect to injection rate exhibit a remarkably similar pattern.

Nevertheless, the effect of injection rate on hydrogen storage exhibits considerable variation across different injection rate ranges, which can be clearly seen in Figure 11(b). The shift in this effect occurs at an injection rate of 2.3×10^6 m^3/day, which serves as a critical threshold. For injection rates below this value, the storage ratio demonstrates a near-linear growth trend as the injection rate increases, with a slope of about 4.98 %/($10^6$$m^3$/day). However, when the injection rate surpasses this value, the rate of increase in the storage ratio slows significantly. This is primarily due to the fact that at low injection rates, the volume of hydrogen injected is small, and the existing CH_4 and CO_2 in the reservoir do not exert a significant buffering effect. As the hydrogen injection rate rises, the amount of hydrogen entering the reservoir increases markedly, thereby enhancing the compression of the pre-existing CO_2 and CH_4. The compressed CO_2 and CH_4 in the reservoir behave like a balloon shell, restricting the diffusion of subsequently injected hydrogen.

Figure 12 illustrates the maximum pore pressure corresponding to different injection rates. As observed in Figure 12, the maximum pore pressure in the model increases rapidly when the injection rate exceeds 1.75×10^6 m^3/day. In any case, the maximum pore pressure observed across all cases is consistently lower than the fracture pressure, indicating a safe operational margin. Given the default investigation conditions, it remains feasible to moderately increase the injection rate to further improve the effectiveness of hydrogen storage.

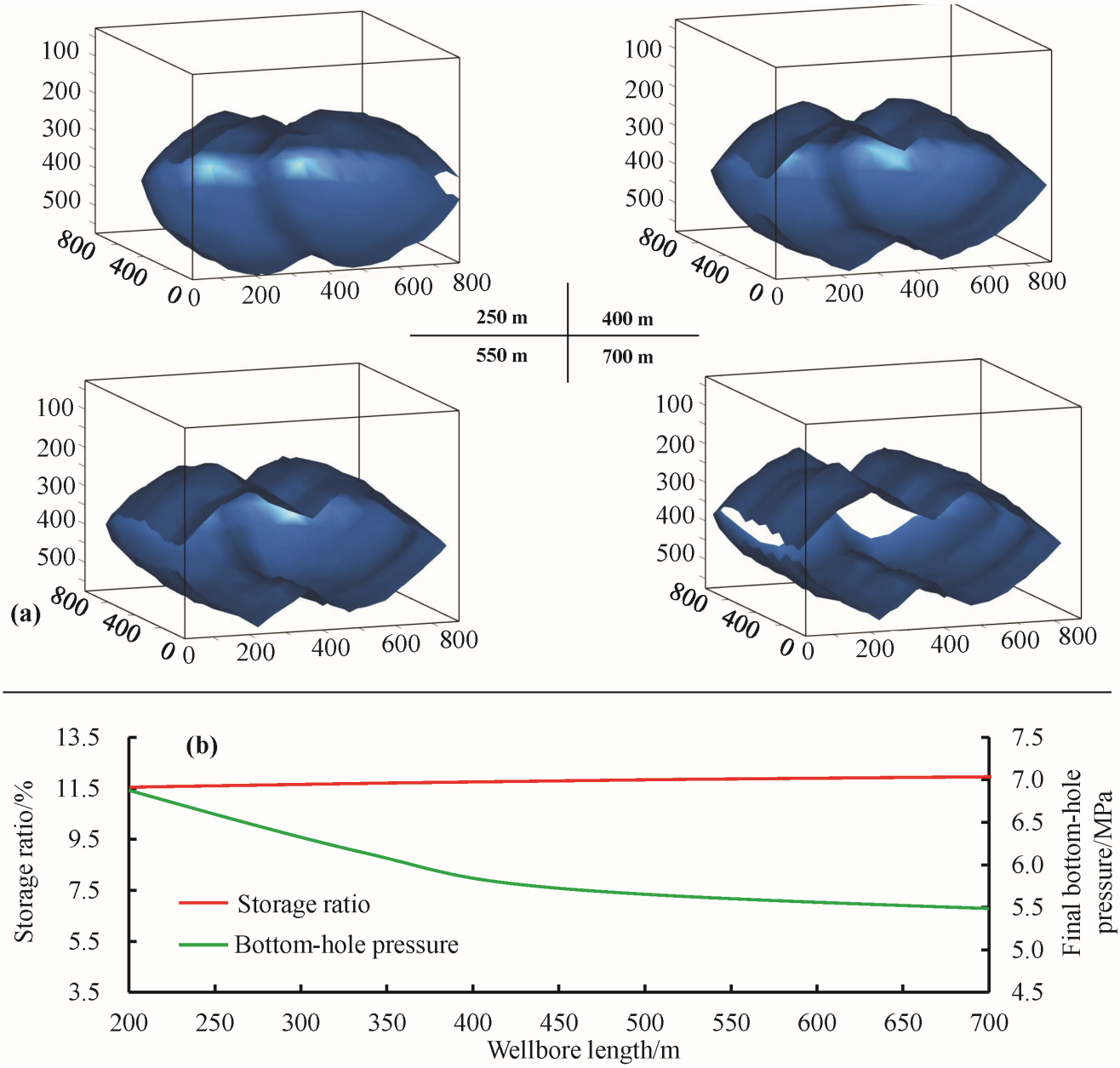


Figure 13. Effect of injection section length on hydrogen storage. (a) Boundary of the final hydrogen distribution area; (b) Storage ratio.

4.3 Effect of wellbore length

As mentioned above, when the total injection rate remains constant, the maximum pore pressure can be regulated by adjusting the wellbore length of the injection section. This adjustment helps ensure the safety of the injection operation and the stability of hydrogen storage. For this purpose, the storage behavior of hydrogen was analyzed for injection section lengths of 250 m, 400 m, 550 m, and 700 m.

Figure 13 illustrates the effect of injection section length (i.e. wellbore length) on storage ratio of the depleted reservoir. As can be seen in Figure 13, when the wellbore length is short, the injected hydrogen must diffuse into the formation through a limited contact area, thereby constraining its distribution. In this case, the injected hydrogen accumulates near the front boundary of the model and exhibits a wide distribution along the longitudinal direction. The limited injection volume per unit time concentrated over a small injection area inevitably results in elevated bottom-hole pressure. When the section length for hydrogen injection is only 250m, the bottom-hole pressure is 6.97MPa, and the storage ratio is 11.5%. As the wellbore length used for hydrogen injection increases, the injected hydrogen penetrates the reservoir across a large surface area of wellbore. As a result, the amount of hydrogen injected per

unit area of the wellbore is reduced, and the final hydrogen distribution area becomes elongated and flat. As a consequence, the injection pressure at the bottom of the wellbore decreases accordingly. When the section length for hydrogen injection is 700 m, the hydrogen injection section almost traverses the full horizontal dimension of the model. Under this operating condition, the bottom-hole pressure decreases to 5.47 MPa, while the storage ratio increases only slightly to 11.98% (see Figure 13(b)). The limited impact of wellbore length on storage ratio can be attributed to the fact that an extended wellbore alters the hydrogen distribution pattern from a wide, circular region to an elongated, flattened configuration. Due to the homogeneous and isotropic nature of sediment permeability in the model, the spatial volume of hydrogen distribution remains largely unchanged with varying wellbore lengths.

Figure 14 illustrates the relationship between wellbore length and the maximum pore pressure within the investigation model. As observed in Figure 14, an increase in wellbore length for hydrogen injection results in a gradual decrease in the maximum pore pressure within the model. Moreover, this decreasing trend in maximum pore pressure is significantly amplified when the wellbore length is shorter than 400 m. For wellbore lengths greater than 400 m, the maximum pore pressure exhibits minimal variation with further increases in length. However, the primary purpose of Figure 14 is to support the design of hydrogen injection operations. From Figure 14, it can be observed that the maximum pore pressure in the model exceeds the fracture pressure only when the wellbore length used for hydrogen injection is shorter than 220 m. Such operation conditions pose environmental risks, as they may cause fracturing within the reservoir, thereby leading to the potential leakage of stored H_2, CO_2, and CH_4. Accordingly, it is advisable to avoid designing the hydrogen injection wellbore section with a length less than 220 m. Furthermore, to enhance the efficiency of future hydrogen recovery, it is recommended to avoid designing an excessively short wellbore section for injection.

5 Conclusions and future works

In this study, a mathematical model was developed to simulate hydrogen injection into a depleted gas reservoir with a certain amount of pre-stored CO_2. Based on this model, the evolution characteristics of parameters such as pore pressure and the mole

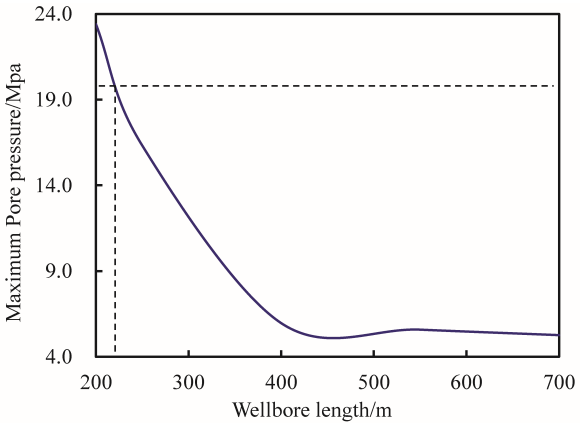


Figure 14. Variation curve of the maximum pore pressure with wellbore length.

fractions of various components (i.e. H_2, CO_2 and CH_4) were analyzed. Subsequently, the effects of injection rate, reservoir permeability, and wellbore length on the hydrogen injection process were systematically discussed. The main conclusions are as follows:

(1) The simulation results obtained in this study show strong consistency with those reported by Lu et al. [28]. This consistency verifies the reliability and applicability of the developed model and methodology for simulations of hydrogen injection and storage in depleted gas reservoir.

(2) The buffering capacity of CH_4 and CO_2 initially present in the depleted gas reservoir becomes increasingly evident as hydrogen injection proceeds, reaching a more significant level during the later stages. As a result of this buffering effect, the expansion of the hydrogen distribution volume within the reservoir gradually slows down.

(3) For low-permeability reservoirs, it is imperative to meticulously balance hydrogen injection efficiency with reservoir stability to optimize hydrogen storage operations. For the default investigation conditions in this study, when reservoir permeability falls below 0.2 mD, it is essential to appropriately adjust the injection rate or the wellbore length to mitigate the risk of gas leakage.

(4) Compared to wellbore length, the injection rate exerts a greater influence on hydrogen storage, primarily because higher rates result in greater volumes of hydrogen being injected, necessitating more available pore space. However, the wellbore length poses a greater risk to reservoir sealing.

The present work represents a foundational study, and

further comprehensive investigations are encouraged to validate and extend these results. Two potential research directions are proposed to guide future studies, with the aim of supporting hydrogen storage projects and contributing to the sustainable development of human society.

(1) The simulation of the alternating hydrogen injection and extraction process is designed to reproduce the peak-shaving behavior of hydrogen production and demand. Such a simulation may better reflect the purpose and intended function of hydrogen storage.

(2) Although the injection of hydrogen plays a key role, the capacity to effectively develop and exploit stored hydrogen is of greater significance. Another idea identified by the authors is the exploration of how different factors affect the purity of hydrogen recovered from storage reservoir. In addition, optimizing the coordination between injection project and recovery project is also essential to maximize the purity of the extracted hydrogen.

Data Availability Statement

Data will be made available on request.

Funding

This work was supported without any funding.

Conflicts of Interest

The authors declare no conflicts of interest.

Ethical Approval and Consent to Participate

Not applicable.

References

[1] Kovač, A., Paranos, M., & Marciuš, D. (2021). Hydrogen in energy transition: A review. *International Journal of Hydrogen Energy, 46*(16), 10016-10035. [CrossRef]

[2] Yue, M., Lambert, H., Pahon, E., Roche, R., Jemei, S., & Hissel, D. (2021). Hydrogen energy systems: A critical review of technologies, applications, trends and challenges. *Renewable and Sustainable Energy Reviews, 146*, 111180. [CrossRef]

[3] Gabrielli, P., Poluzzi, A., Kramer, G. J., Spiers, C., Mazzotti, M., & Gazzani, M. (2020). Seasonal energy storage for zero-emissions multi-energy systems via underground hydrogen storage. *Renewable and Sustainable Energy Reviews, 121*, 109629. [CrossRef]

[4] Epelle, E. I., Obande, W., Udourioh, G. A., Afolabi, I. C., Desongu, K. S., Orivri, U., ... & Okolie, J. A. (2022). Perspectives and prospects of underground hydrogen storage and natural hydrogen. *Sustainable Energy & Fuels, 6*(14), 3324-3343. [CrossRef]

[5] Caglayan, D. G., Weber, N., Heinrichs, H. U., Linßen, J., Robinius, M., Kukla, P. A., & Stolten, D. (2020). Technical potential of salt caverns for hydrogen storage in Europe. *International Journal of Hydrogen Energy, 45*(11), 6793-6805. [CrossRef]

[6] Tarkowski, R. (2019). Underground hydrogen storage: Characteristics and prospects. *Renewable and Sustainable Energy Reviews, 105*, 86-94. [CrossRef]

[7] Michael, K., Golab, A., Shulakova, V., Ennis-King, J., Allinson, G., Sharma, S., & Aiken, T. (2010). Geological storage of CO2 in saline aquifers—A review of the experience from existing storage operations. *International journal of greenhouse gas control, 4*(4), 659-667. [CrossRef]

[8] Bachu, S. (2015). Review of CO2 storage efficiency in deep saline aquifers. *International Journal of Greenhouse Gas Control, 40*, 188-202. [CrossRef]

[9] Wei, B., Wang, B., Li, X., Aishan, M., & Ju, Y. (2023). CO2 storage in depleted oil and gas reservoirs: A review. *Advances in Geo-Energy Research, 9*(2), 76–93. [CrossRef]

[10] Askarova, A., Mukhametdinova, A., Markovic, S., Khayrullina, G., Afanasev, P., Popov, E., & Mukhina, E. (2023). An overview of geological CO2 sequestration in oil and gas reservoirs. *Energies, 16*(6), 2821. [CrossRef]

[11] Tyne, R. L., Barry, P. H., Lawson, M., Byrne, D. J., Warr, O., Xie, H., Hillegonds, D. J., Formolo, M., Summers, Z. M., Skinner, B., Eiler, J. M., & Ballentine, C. J. (2021). Rapid microbial methanogenesis during CO2 storage in hydrocarbon reservoirs. *Nature, 600*(7890), 670–674. [CrossRef]

[12] Deng, P., Ma, H., Song, J., Peng, X., Zhu, S., Xue, D., Jiang, L., & Chen, Z. (2025). Carbon dioxide as cushion gas for large-scale underground hydrogen storage: Mechanisms and implications. *Applied Energy, 388*, 125622. [CrossRef]

[13] Saeed, M., Jadhawar, P., & Bagala, S. (2023). Geochemical effects on storage gases and reservoir rock during underground hydrogen storage: a depleted North Sea oil reservoir case study. *Hydrogen, 4*(2), 323–337. [CrossRef]

[14] Amid, A., Mignard, D., & Wilkinson, M. (2016). Seasonal storage of hydrogen in a depleted natural gas reservoir. *International journal of hydrogen energy, 41*(12), 5549-5558. [CrossRef]

[15] Dehghani, M. R., Ghazi, S. F., & Kazemzadeh, Y. (2024). Interfacial tension and wettability alteration during hydrogen and carbon dioxide storage in depleted gas reservoirs. *Scientific Reports, 14*(1), 11594. [CrossRef]

[16] Liu, K., Zhu, W., & Pan, B. (2024). Feasibility of hydrogen storage in depleted shale gas reservoir: A numerical investigation. *Fuel, 357*, 129703. [CrossRef]

[17] Muhammed, N. S., Haq, B., Al Shehri, D., & ... (2023). Role of methane as a cushion gas for hydrogen storage in depleted gas reservoirs. *International Journal of Hydrogen Energy, 48*(76), 29663–29681. [CrossRef]

[18] Kanaani, M., Sedaee, B., & Asadian-Pakfar, M. (2022). Role of cushion gas on underground hydrogen storage in depleted oil reservoirs. *Journal of Energy Storage, 45*, 103783. [CrossRef]

[19] He, Y., Xie, Y., Qiao, Y., Qin, J., & Tang, Y. (2024). Estimation of underground hydrogen storage capacity in depleted gas reservoirs using CO2 as cushion gas. *Applied Energy, 375*, 124093. [CrossRef]

[20] Zeng, L., Sarmadivaleh, M., Saeedi, A., Chen, Y., Zhong, Z., & Xie, Q. (2023). Storage integrity during underground hydrogen storage in depleted gas reservoirs. *Earth-Science Reviews, 247*, 104625. [CrossRef]

[21] Muhammed, N. S., Haq, B., Al Shehri, D., Al-Ahmed, A., Rahman, M. M., & Zaman, E. (2022). A review on underground hydrogen storage: Insight into geological sites, influencing factors and future outlook. *Energy Reports, 8*, 461-499. [CrossRef]

[22] Perera, M. S. A. (2023). A review of underground hydrogen storage in depleted gas reservoirs: Insights into various rock-fluid interaction mechanisms and their impact on the process integrity. *Fuel, 334*, 126677. [CrossRef]

[23] Zivar, D., Kumar, S., & Foroozesh, J. (2021). Underground hydrogen storage: A comprehensive review. *International journal of hydrogen energy, 46*(45), 23436-23462. [CrossRef]

[24] Mirhasan Hosseini, S. I., Fahimpour, J., Ali, M., & Keshavarz, A. (2022). Capillary Sealing Efficiency Analysis of Caprocks: Implication for Hydrogen Geological Storage. *Energy & Fuels, 36*(7), 4065–4075. [CrossRef]

[25] Chabab, S., Théveneau, P., Coquelet, C., Corvisier, J., & Paricaud, P. (2020). Measurements and predictive models of high-pressure H2 solubility in brine (H2O+ NaCl) for underground hydrogen storage application. *International Journal of Hydrogen Energy, 45*(56), 32206-32220. [CrossRef]

[26] Hashemi, L., Glerum, W., Farajzadeh, R., & Hajibeygi, H. (2021). Contact angle measurement for hydrogen/brine/sandstone system using captive-bubble method relevant for underground hydrogen storage. *Advances in Water Resources, 154*, 103964. [CrossRef]

[27] Lysyy, M., Fernø, M., & Ersland, G. (2021). Seasonal hydrogen storage in a depleted oil and gas field. *International Journal of Hydrogen Energy, 46*(49), 25160-25174. [CrossRef]

[28] Lu, J., Muhammed, N. S., Okolie, J. A., & Epelle, E. I. (2025). A sensitivity study of hydrogen mixing with cushion gases for effective storage in porous media. *Sustainable Energy & Fuels, 9*(5), 1353–1370. [CrossRef]

[29] Flesch, S., Pudlo, D., Albrecht, D., Jacob, A., & Enzmann, F. (2018). Hydrogen underground storage—Petrographic and petrophysical variations in reservoir sandstones from laboratory experiments under simulated reservoir conditions. *International Journal of Hydrogen Energy, 43*(45), 20822-20835. [CrossRef]

[30] Zamehrian, M., & Sedaee, B. (2022). Underground hydrogen storage in a naturally fractured gas reservoir: The role of fracture. *International Journal of Hydrogen Energy, 47*(93), 39606–39618. [CrossRef]

[31] Zeng, L., Sander, R., Chen, Y., & Xie, Q. (2024). Hydrogen storage performance during underground hydrogen storage in depleted gas reservoirs: a review. *Engineering, 40*, 211–225. [CrossRef]

[32] Heinemann, N., Alcalde, J., Miocic, J. M., Hangx, S. J., Kallmeyer, J., Ostertag-Henning, C., ... & Rudloff, A. (2021). Enabling large-scale hydrogen storage in porous media–the scientific challenges. *Energy & Environmental Science, 14*(2), 853-864. [CrossRef]

[33] Okere, C. J., Sheng, J. J., & Ejike, C. (2024). Evaluating reservoir suitability for large-scale hydrogen storage: a preliminary assessment considering reservoir properties. *Energy Geoscience, 5*(4), 100318. [CrossRef]



Jingjuan Wu is a full-time faculty member at the School of Materials Science and Engineering, Henan Polytechnic University, Jiaozuo, China. Her research interests include the efficient development of unconventional hydrocarbon resources (such as shale gas, natural gas hydrate), CCUS and hydrogen storage. Wu Jingjuan earned her master's degree from Henan University of Science and Technology, Luoyang, China in 2017, and joined the School of Materials Science and Engineering at Henan Polytechnic University in 2020. (Email: wjj2020@hpu.edu.cn)



Ubedullah Ansari is a lecturer at Mehran University of Engineering & Technology, Jamshoro, Pakistan. He holds a bachelor's and master's degree in petroleum engineering from Mehran University of Engineering & Technology, Jamshoro, Pakistan, and a doctoral degree in petroleum engineering from China University of Petroleum (East China), Qingdao, China. Ansari has experience working with SPE Mehran Student Chapter, the first SPE student chapter of Pakistan, as treasurer and faculty advisor. He has extensive experience in oil- and gas-field-related collaborative and independent research projects. In terms of academic part-time work, he serves as an Associate Editor for the Mehran University Research Journal of Engineering and Technology and as a Review Editor for Frontiers in Earth Science. (Email: ubedullah.ansari@faculty.muet.edu.pk)